Supporting Material for

Microscopic origin of gating current fluctuations in a potassium channel voltage sensor

J. Alfredo Freites,[*] Eric V. Schow,[*] Stephen H. White,[†] and Douglas J. Tobias[*]

[*]Department of Chemistry and [†]Department of Physiology and Biophysics, University of California, Irvine, CA 92697, USA
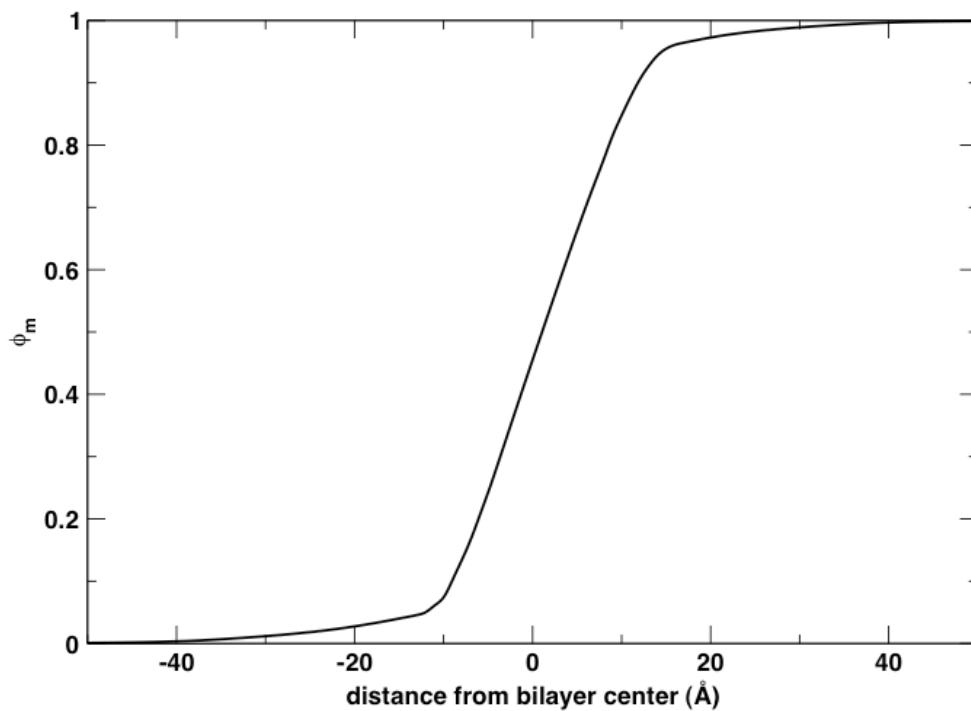
Figure S1. Fractional membrane potential (Φ_m) calculated along a transmembrane axis passing through the center of the the KvAP VSD. The linear potential drop extends of ~23 Å. This profile is taken from a linearized Poisson-Boltzmann calculation reported in (1).
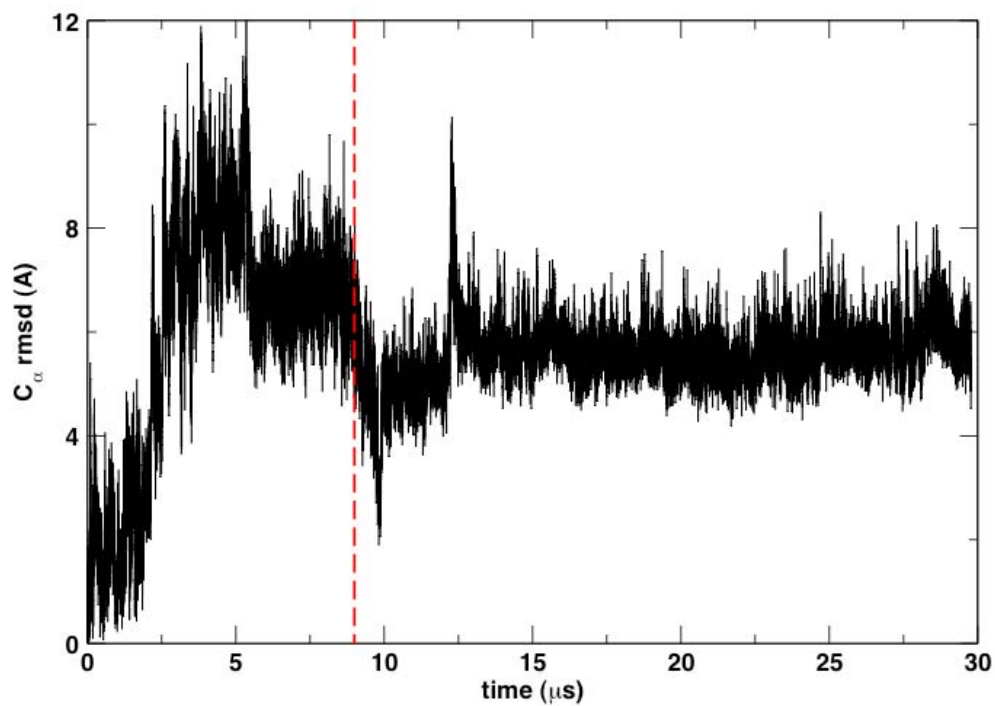
Figure S2. Conformational dynamics of the S3b-S4 paddle motif, as the C_α rmsd from the VSD initial configuration with respect to S1-S2, along the simulation trajectory. The broken red line indentifies the switch from the depolarizing potential (+120 mV) to the hyperpolarizing potential (-120 mv).
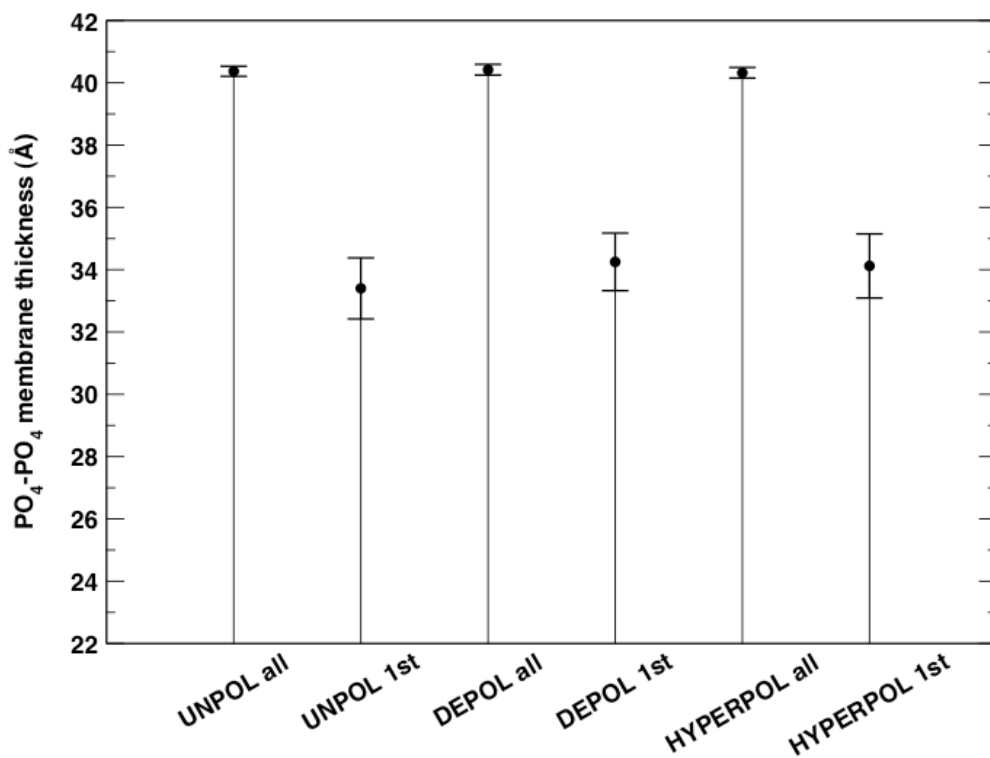
Figure S3. Lipid bilayer thickness measured as mean distance between lipid phosphate groups in opposite leaflets. Values are shown for all lipids and those in the first VSD solvation shell (cutoff of 4.5 Å) for the unpolarized simulation (Fig. S5), and the simulation under depolarizing and hyperpolarizing potentials (Fig. 1). No significant differences due to the action of the applied membrane potention are observed. Error bars indicate the statistical uncertainty at the 95% confidence level.
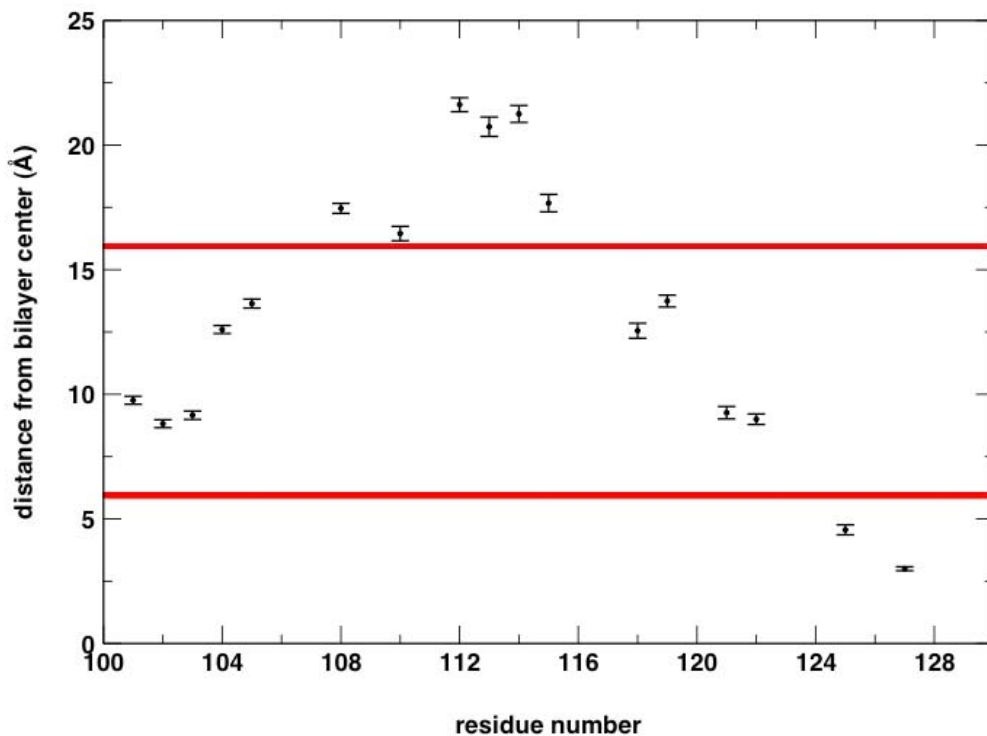
Figure S4. Interpretation of the KvAP biotin-avidin accessibility data for the S3b-S4 paddle motif (2, 3) in terms of positions of the Cα atoms along the transmembrane direction measured as mean values over the last 4.5 µs of trajectory under a depolarizing potential. The upper red band represents the location of the extracellular interface (as the mean of the lipid carbonyl distribution) and the lower band represents the effective length of the biotin tether (10 Å). Residues whose Cα atoms fall within the two bands or over the upper band are considered to be accessible from the extracellular side, and residues located under the lower band are considered not to be accessible from the extracellular side under a depolarizing potential. The simulation data is in complete agreement with the experimental results reported in (2, 3).
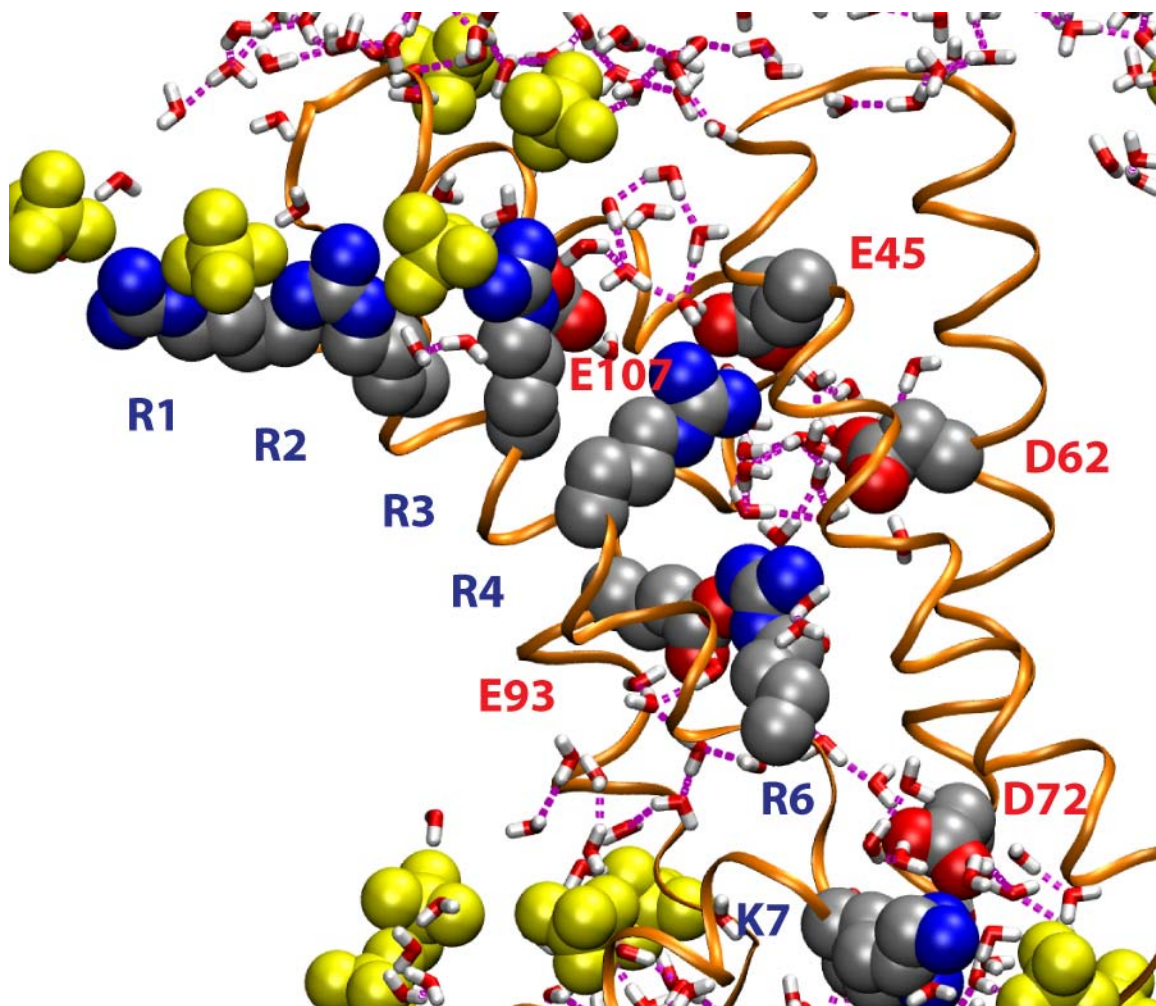
Figure S5. VSD configuration snapshot from a 5 μs unpolarized control simulation (after 4.2 μs). Molecular representations and color scheme are as in Fig. 1. The only significant change with respect to the initial configuration (reported in (4)) is the conversion of the R6-D62 salt-bridge to a water-mediated interaction and the formation of a water-mediated interaction between R6 and E93.
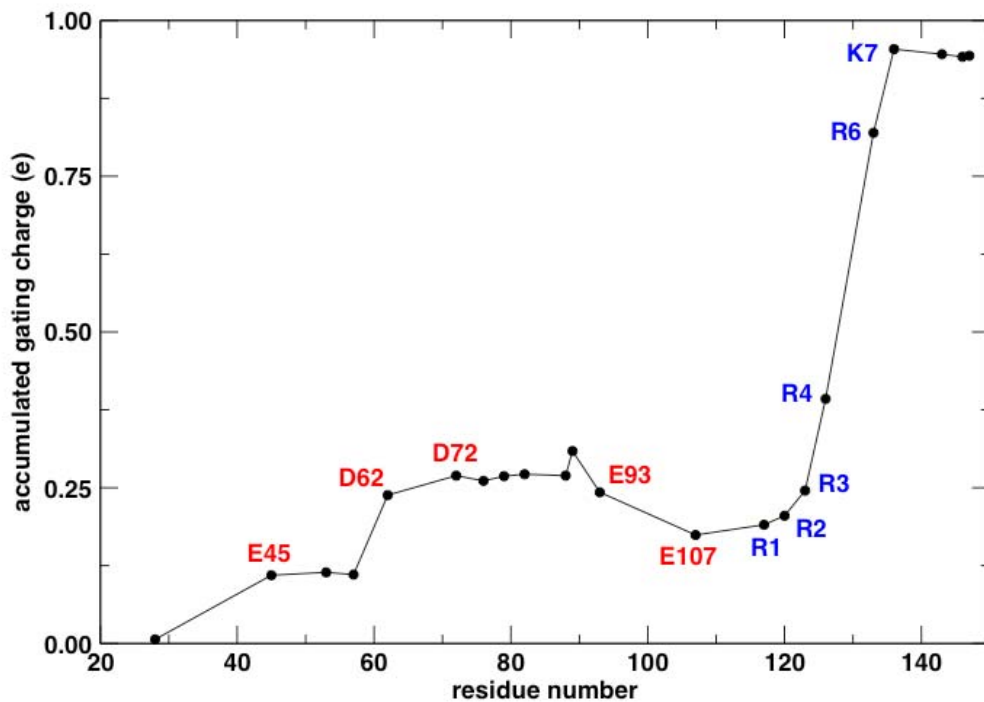
Figure S6. Per-residue contributions to the gating charge. The gating charge associated to each VSD basic or acidic side chain was calculated as difference between the average charge displacement over the last 3 μs of the depolarized trajectory and the average charge displacement 16 μs of the hyperpolarized trajectory. Conserved positions for acidic side chains in S1-S3 and for basic side chains in S4 and the S4-S5 linker are labeled as in Fig. 1. Also indicated is E107 a side chain in S3b that forms salt-bridges with R3 and R4.
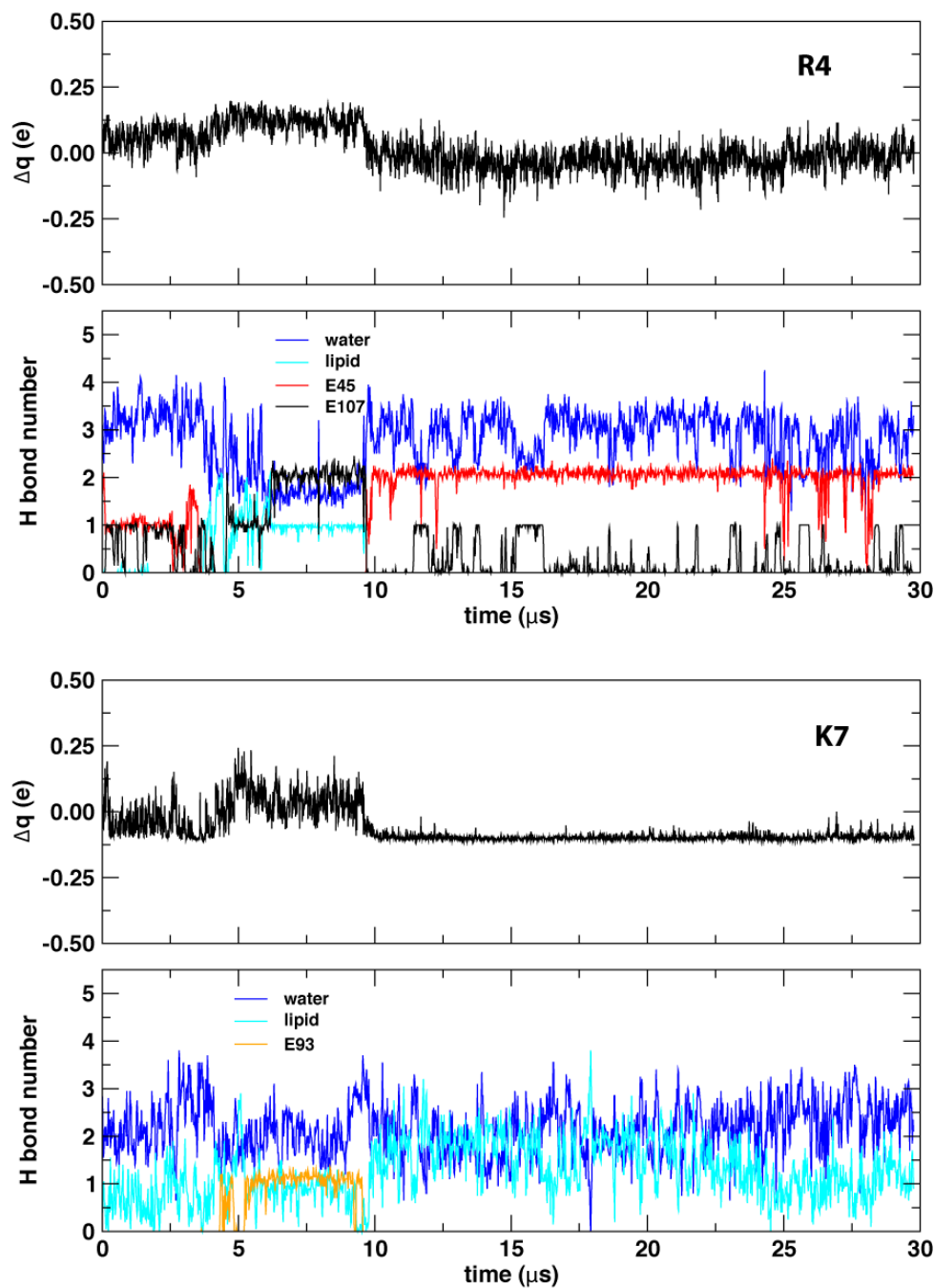
Figure S7. Evolution of the charge displacement and solvation environment for R4 (top two graphs) and K7 (bottom two graphs). Similar to R6, the contributions to the total charge displacement for R4 and K7 follow closely the changes in their solvation environments. R4, besides forming salt-bridges and water-mediated interactions with conserved acidic side chains (E45 and D62), also forms a flickering salt-bridge with E107 (in S3b) which is not part of the set of S1-S3 conserved positions for acidic side chains in Kv channels.
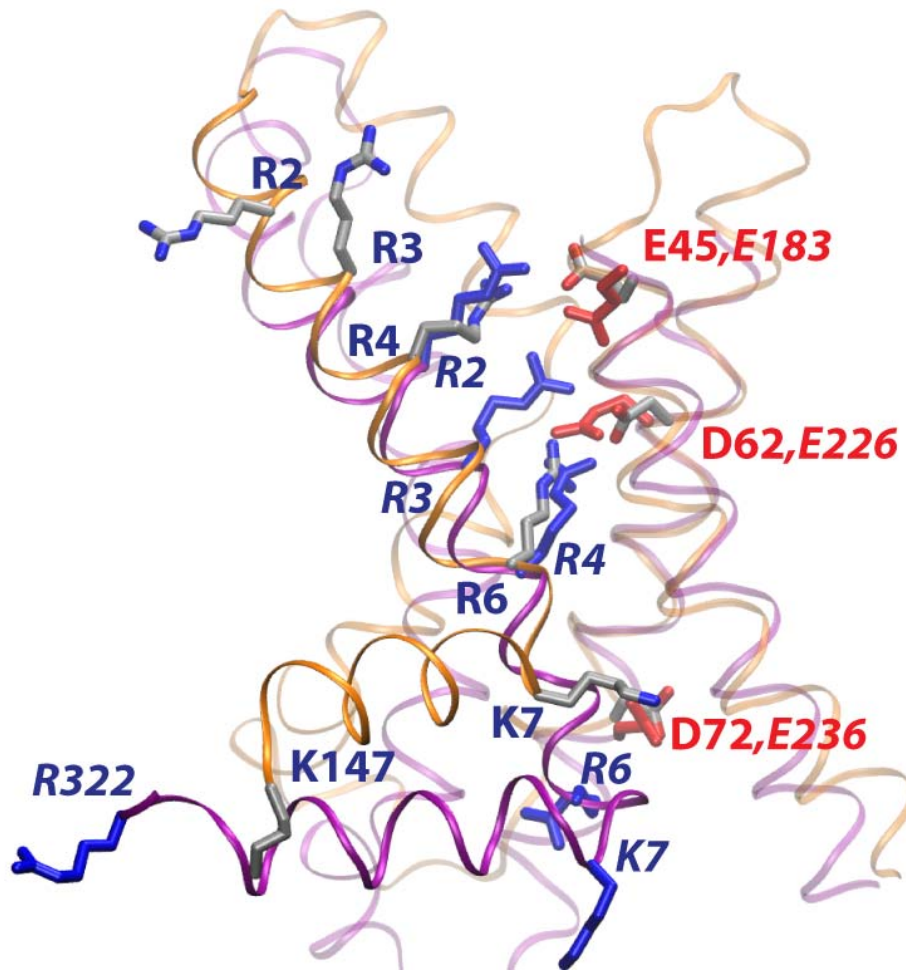
Figure S8. Comparison of the KvAP VSD structure (orange; residues 24 to 147 of the KvAP full channel model proposed by Lee et al. (5)) with the X-ray crystal structure of the Kv1.2 paddle-chimera channel VSD (purple; residues 162 to 322) (6). The superposition was performed by minimizing the backbone rmsd of the S1-S2 transmembrane segments. The difference in length of the S4 segments in both structures causes an apparent relative shift on the spatial location of the S4 basic side chains. Thus, the R6 position in KvAP and the R4 position in Kv1.2 share a common location close to the VSD constriction region separating the extracellular and intracellular crevices. Note that the S1-S2 alignment places the S4-S5 linker C-terminal backbones at similar locations along the transmembrane direction. KvAP side chains are colored by atom type (cf. Fig. 1) and those from Kv1.2 are colored by residue type (basic, blue; acidic, red). KvAP residue numbers are indicated in plain font, and Kv1.2 residue numbers are in italics. The Kv1.2 S1-S2 loop was omitted for clarity.
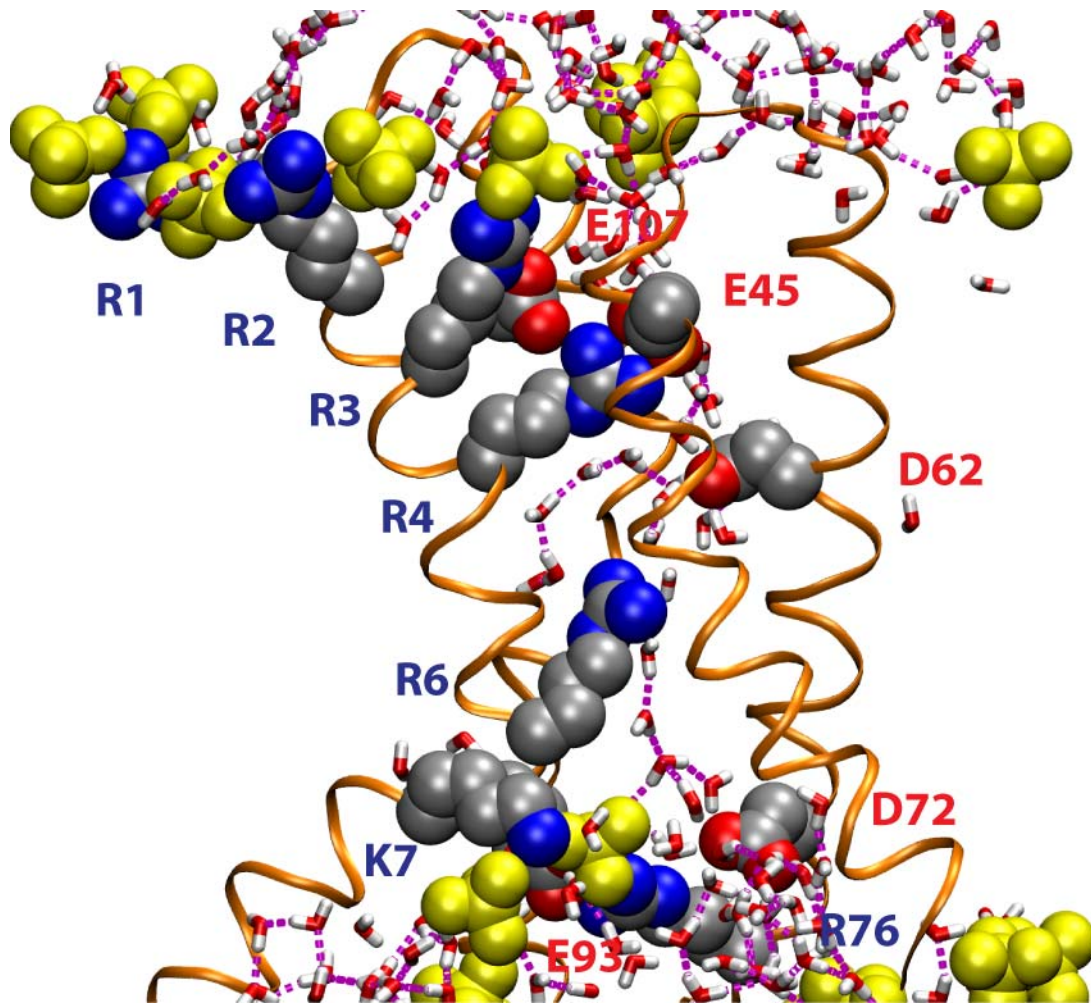
Figure S9. VSD configuration snapshot from the end of a 14 µs trajectory under a -120 mV hyperpolarizing potential started from an unpolarized configuration. In contrast to the configuration of the charged side chains at the end of the hyperpolarized trajectory started from a depolarized configuration (Fig. 1C), the R6 center of charge remains at center of the VSD (as in the unpolarized configuration, cf. Fig. S5) and K7 is exposed to the VSD intracellular crevice. Molecular representations and color scheme are as in Fig. 1.

Methods

Simulation system. The initial atomistic model of the unpolarized KvAP VSD corresponds to residues 24 to 147 of the KvAP full channel model proposed by Lee et al. (5). The initial simulation system configuration was derived from the end of a previously equilibrated, unpolarized simulation of the KvAP VSD in a POPC bilayer in excess water (4). The system consisted of 10,048 waters, 232 lipids, 2 chloride counterions, and 1 VSD, for a total of 63,247 atoms.

Molecular dynamics simulations. The μs-timescale simulations were performed on Anton, a special-purpose computer for molecular dynamics simulations of biomolecules (7). The system was equilibrated for 12 ns using the Desmond Molecular Dynamics System, version 2.4 (D. E. Shaw Research, New York, NY, 2008) on a conventional high performance cluster before being transferred to Anton. The CHARMM22 (8) and CHARMM36 (9) force fields were used for the protein and lipids, respectively, and the TIP3P model was used for water. A reversible multiple-timestep algorithm was employed to integrate the equations of motion with a time step of 6 fs for the long-range non-bonded forces, and 2 fs for short-range non- bonded and bonded forces. All bond lengths involving hydrogen atoms were held fixed using the SHAKE algorithm. The k-space Gaussian split Ewald method (10) with a 32 x 32 x 32 grid was used to calculate long-range electrostatic interactions. A cutoff of 14 Å was used for the Lennard-Jones and short-range electrostatic interactions. The simulations were performed at constant temperature (300 K) and pressure (1 atm), using a Berendsen thermostat and semi-isotropic Berendsen barostat. Analyses and visualization were performed with VMD 1.9 (11).

Membrane potential and gating charge. To model the applied membrane potential, we imposed a constant electric field with a magnitude equal to 120 mV/23 Å. The specific value for the thickness of the dielectric barrier was taken from a linearized Poisson-Boltzmann calculation of the electrostatic potential along a transmembrane axis passing through the center of the VSD (see Fig. S1), as previously described (1). The total charge displacement with respect to the initial configuration (Δq) was calculated as

$$\Delta q = \sum_i q_i \left(\Phi_m[z_i(t)] - \Phi_m[z_i(0)] \right)$$

where t is time, Φ_m is the fractional membrane potential shown in Fig. S1, and z_i and q_i are the position along the transmembrane direction and the partial charge of the ith atom, respectively. The sum was taken over the partial charges of the atoms that constitute the centers of charge of all the VSD basic and acidic side chains. The gating-charge displacement (Q) between the depolarized and hyperpolarized trajectories was calculated as

$$Q = \langle \Delta q \rangle_d - \langle \Delta q \rangle_h$$

where $< \Delta q >_d$ is the average charge displacement over the last 3 μs of the depolarized trajectory and $< \Delta q >_h$ is the average charge displacement over the last 16 μs of the hyperpolarized trajectory.

References

1. Krepkiy, D., M. Mihailescu, J. A. Freites, E. V. Schow, D. L. Worcester, K. Gawrisch, D. J. Tobias, S. H. White, and K. J. Swartz. 2009. Structure and hydration of membranes embedded with voltage-sensing domains. *Nature* 462:473-479.
2. Jiang, Y. X., V. Ruta, J. Y. Chen, A. Lee, and R. MacKinnon. 2003. The principle of gating charge movement in a voltage-dependent K$^+$ channel. *Nature* 423:42-48.
3. Ruta, V., J. Chen, and R. MacKinnon. 2005. Calibrated measurement of gating-charge arginine. *Cell* 123:463-475.
4. Freites, J. A., D. J. Tobias, and S. H. White. 2006. A voltage-sensor water pore. *Biophys. J.* 91:L90-L92.
5. Lee, S.-Y., A. Lee, J. Chen, and R. MacKinnon. 2005. Structure of the KvAP voltage-dependent K$^+$ channel and its dependence on the lipid membrane. *Proc. Natl. Acad. Sci. U.S.A.* 102:15441-15446.
6. Long, S. B., X. Tao, E. B. Campbell, and R. Mackinnon. 2007. Atomic structure of a voltage-dependent K$^+$ channel in a lipid membrane-like environment. *Nature* 450:376-382.
7. Shaw, D. E., M. M. Deneroff, R. O. Dror, J. S. Kuskin, R. H. Larson, J. K. Salmon, C. Young, B. Batson, K. J. Bowers, J. C. Chao, M. P. Eastwood, J. Gagliardo, J. P. Grossman, C. R. Ho, D. J. Lerardi, I. Kolossváry, J. L. Klepeis, T. Layman, C. McLeavey, M. A. Moraes, R. Mueller, E. C. Priest, Y. Shan, J. Spengler, M. Theobald, B. Towles, and S. C. Wang. 2007. Anton, a special-purpose machine for molecular dynamics simulation. *Proc. 34th Annu. Internat. Sym. Computer Architect.*
8. MacKerell, A. D., Jr., M. Feig, and C. L. Brooks, II. 2004. Extending the treatment of backbone energetics in protein force fields: Limitations of gas-phase quantum mechanics in reproducing conformational distributions in molecular dynamics simulations. *J. Comput. Chem.* 25:1400-1415.
9. Klauda, J. B., R. M. Venable, J. A. Freites, J. W. O'Connor, D. J. Tobias, C. Mondragon-Ramirez, I. Vorobyov, A. D. MacKerell, Jr., and R. W. Pastor. 2010. Update of the CHARMM all-atom additive force field for lipids: validation on six lipid types. *J. Phys. Chem. B* 114:7830-7843.
10. Shan, Y., J. L. Klepeis, M. P. Eastwood, R. O. Dror, and D. E. Shaw. 2005. Gaussian split Ewald: a fast Ewald mesh method for molecular simulation. *J. Chem. Phys.* 122:054101-054101 to 054101-054113.
11. Humphrey, W., W. Dalke, and K. Schulten. 1996. VMD: Visual molecular dynamics. *J. Mol. Graph.* 14:33-38.